Crystalline and amorphous structures of Ge–Sb–Te nanoparticles

Gyeong-Su ParkJi-Hwan Kwon and Miyoung KimH. R. Yoon and W. JoT. K. Kim and Jian-Min ZuoYoonho Khang

Citation: Journal of Applied Physics **102**, 013524 (2007); doi: 10.1063/1.2752550
View online: http://dx.doi.org/10.1063/1.2752550
View Table of Contents: http://aip.scitation.org/toc/jap/102/1
Published by the American Institute of Physics

Crystalline and amorphous structures of Ge–Sb–Te nanoparticles

Gyeong-Su Park
Analytical Engineering Center, Samsung Advanced Institute of Technology, P.O. Box 111, Suwon 440-600, Korea

Ji-Hwan Kwon and Miyoung Kim[a)]
Department of Materials Science and Engineering, Seoul National University, Seoul 151-744, Korea

H. R. Yoon and W. Jo
Department of Physics, Ewha Womans University, Seoul 120-750, Korea

T. K. Kim and Jian-Min Zuo
Department of Materials Science and Engineering, University of Illinois at Urbana-Champaign, Illinois 61801

Yoonho Khang
Semiconductor Device and Material Lab, Samsung Advanced Institute of Technology, P.O. Box 111, Suwon 440-600, Korea

(Received 31 January 2007; accepted 29 May 2007; published online 10 July 2007)

We report effects of thermal annealing on the structures of Ge–Sb–Te (GST) nanoparticles synthesized by pulsed laser ablation deposition. The average diameter of the GST nanoparticles is an order of 10 nm. The as-prepared sample contains nanocrystals surrounded by an amorphous phase. Further crystallization occurs during annealing. The structures of the nanocrystals and amorphous phase were studied by electron diffraction and radial distribution function analyses. The results show that the nanoparticles annealed at 100 °C are crystalline, consisting of a mixture of face centered cubic (fcc) and hexagonal $Ge_2Sb_2Te_5$ (dominant). In comparison, the nanoparticles annealed at 200 °C are mostly fcc. The surrounding amorphous phase has similar atomic arrangements to the previously reported amorphous GST thin films. © *2007 American Institute of Physics*. [DOI: 10.1063/1.2752550]

I. INTRODUCTION

Chalcogenide materials have high crystallization rate, high thermal stability, and good reversibility between amorphous and crystalline phases. They are widely used as optical disk storage materials. Recently, chalcogenides have attracted considerable interest as the material for nonvolatile phase change random access memory (PCRAM). Studies so far have shown that $Ge_2Sb_2Te_5$ (GST) has the best combination of electric and phase changing characteristics for PCRAM applications.[1–3] The structure of a GST material is critical to its performance. Luo and Wuttig pointed out that the rocksalt structure is preferred in high-speed phase change materials, since it enables fast crystallization due to its simplicity.[4] In GST, the electrical resistivity changes drastically when the structure changes from amorphous to the metastable face-centered cubic (fcc) structure at 140 °C, and from the FCC to the stable hexagonal structure at 370 °C.[5]

For PCRAM applications, fast and reversible phase transformation is obtained by Joule heating using electrical pulses. The application of a current with a high magnitude and a fast falling edge leads to amorphization through the processes of melting followed by quenching (reset), while a current with a long and moderate magnitude induces crystallization by the annealing process in the PCRAM (set).[6,7] The scalability of memory capacity depends on how one can effectively reduce the critical reset currents required for switching from the crystalline to amorphous phase. There have been several proposals for the reduction of the reset current.[8–10] One approach is to replace GST nanoparticles with the case where thin films are conventionally used.[11,12] However, there is little structural information about these nanoparticles, especially regarding their structural phases.

Herein, we report the structure characterization of GST nanoparticles synthesized by pulsed laser ablation. These particles show a reduction of the reset current by a factor of 1000 compared with that of conventional GST films.[13,14] We investigated the structure of both the amorphous and crystal phases of the GST nanoparticles, using the nanoarea electron diffraction (NED) technique.[15] Radial distribution function (RDF) analyses using NED patterns were performed to identify the local structural changes in the amorphous phase.

II. EXPERIMENT

A sintered GST target of high density was used for laser ablation. The GST nanoparticles were prepared using an ArF (=193 nm) excimer pulsed laser. The laser pulse rate and pulse width were 5 Hz and 20 ns, respectively. The GST nanoparticles were grown on KCl or NaCl crystals in an Ar atmosphere and then thermally treated in a heating furnace at 100 or 200 °C. The nanoparticles were previously characterized by secondary electron microscopy (SEM) and Raman

[a)]Author to whom correspondence should be addressed; electronic mail: mkim@snu.ac.kr.

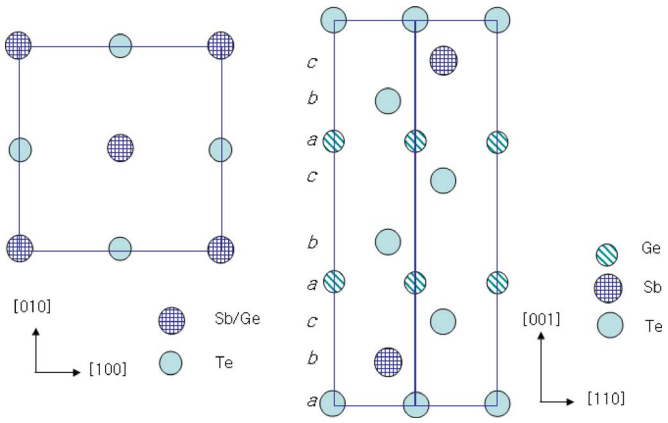

FIG. 1. Atomic structures of $Ge_2Sb_2Te_5$. (Left) The face centered cubic rocksalt structure and (right) the hexagonal structure.

spectroscopy.[16] In this study, the samples were studied using the JEOL-2010F transmission electron microscope installed at the University of Illinois and operated at 200 kV. Electron diffraction measurements of the nanoparticles were carried out in the NED mode with an electron probe having a diameter of 50 nm. The use of a small probe allows for the selection of a thin area for the electron diffraction analysis. Both the amorphous phase and nanoparticles were included within the area of the electron probe. Imaging plates with a large dynamic range and linearity were used to record the NED patterns, and the intensity was analyzed to extract structural information. X-ray energy dispersive spectroscopy (EDS) was used to check the composition of the nanoparticles, and the results obtained confirmed the stoichiometry of the $Ge_2Sb_2Te_5$.[13] The diffraction patterns were recorded from several areas in each sample. Each area contained a few to several tens of nanoparticles.

III. RESULTS AND DISCUSSION

We first review the different crystal structures of GST. The face centered cubic (fcc) GST has a rocksalt structure, with the space group $Fm\text{-}3m$ and a lattice constant of 6.01 Å.[17] There are two sites in the rocksalt structure: one site is fully occupied by Te, and the other site is randomly occupied by Ge or Sb or vacancy. The number of vacancies represents about 20% of the Ge/Sb sites. The structure of the stable hexagonal GST is complex; it consists of nine layers, with each layer containing one of the three atoms in the GST. The stacking sequence of Te–Sb–Te–Ge–Te–Te–Ge–Te–Sb reported by Petrov *et al.* is shown in Fig. 1.[18] The layers follow the fcc close-packing sequence, *abcabc*…, with atomic positions of $(0,0,z_1)$ in a, $(2/3,1/3,z_2)$ in b, and $(1/3,2/3,z_3)$ in c. The lattice constants of this structure are $a=4.22$ Å and $c=16.96$ Å. The recent publication by Kooi and De Hosson[19] suggested the stacking order of Te–Ge–Te–Sb–Te–Te–Sb–Te–Ge, where the positions of Ge and Sb are interchanged and the lattice constants are $a=4.25$ Å and $c=18.27$ Å. Their results were based on electron diffraction. Matsunaga *et al.* suggested another structure consisting of randomly occupied Ge and Sb layers with the lattice constants $a=4.22$ Å and $c=17.24$ Å.[20]

The samples are composed of both amorphous and crystal phases. The size of the nanoparticles does not depend much on the annealing temperatures. The nanoparticle diameters range from 5 to 25 nm.[13,16] Figure 2 shows representative high-resolution transmission electron microscopy (HR-TEM) images recorded from the three samples (group I without annealing, group II with annealing at 100 °C, and group III with annealing at 200 °C). The nanoparticles are approximately spherical and surrounded by an amorphous phase. Examples of the electron diffraction patterns recorded from the three samples are shown in Fig. 3. These diffraction patterns were recorded from areas with a large concentration of nanoparticles; each diffraction pattern was captured from a few tens of nanoparticles. The diffraction patterns consist of hazy rings from the amorphous phase and relatively sharp diffraction spots from the nanocrystals. The diffraction spots are generally sparse and weak in the as-prepared samples (group I) and relative dense and strong in the annealed samples, which indicates an increase in both the crystallite density and size.

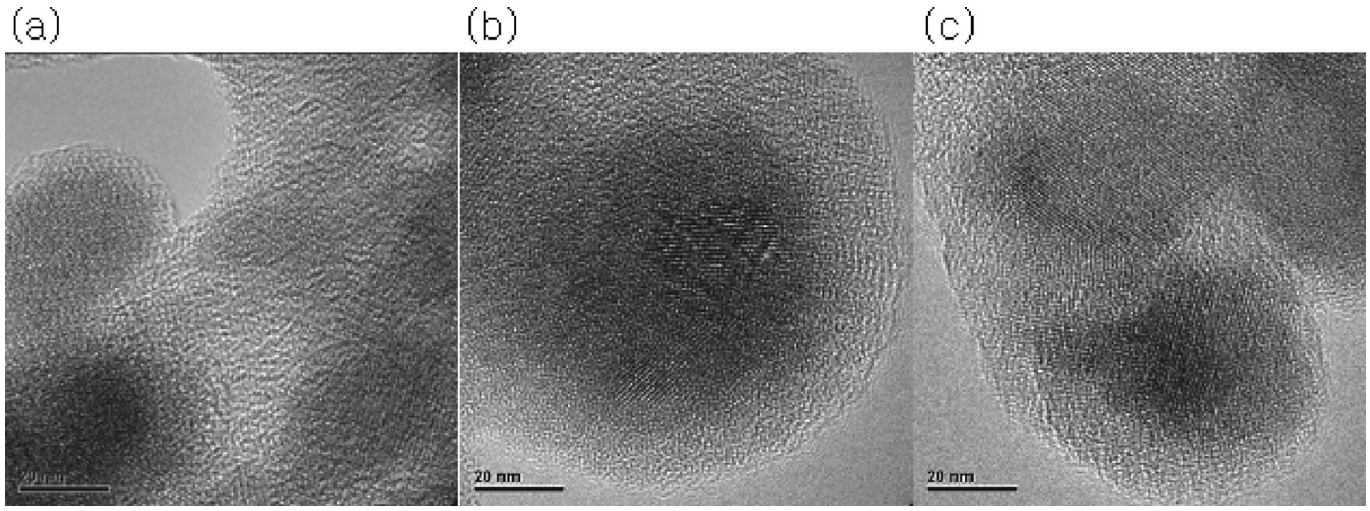

FIG. 2. High-resolution transmission electron microscopy (HREM) images of the three samples of $Ge_2Sb_2Te_5$ nanoparticles synthesized (a) at room temperature, (b) at 100 °C and (c) at 200 °C.

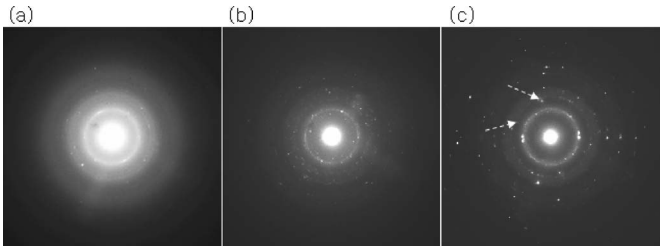

FIG. 3. Electron diffraction patterns of the three samples of $Ge_2Sb_2Te_5$ nanoparticles synthesized (a) at room temperature, (b) at 100 °C and (c) at 200 °C. The diffraction pattern consists of hazy rings from the amorphous phase and diffraction spots from the nanocrystals.

To identify the structural phases in the nanoparticles, we averaged the diffraction patterns to obtain the radial diffraction intensities (Fig. 4). Each figure shows three radial diffraction intensities from three different areas for the purpose of comparison. Among these figures, the solid curves in Fig. 4 were obtained from the diffraction pattern shown in Fig. 3. The scattering vectors defined by $s=\sin(\theta_B)/\lambda$, where θ_B is the Bragg angle and λ is a wavelength of incident electrons accelerated at 200 kV, are listed in the Table I. The radial intensity profile was useful for identifying the dominant phases in the nanoparticles. Some of the weak diffraction spots which can be seen in the diffraction patterns are missing in the radial profile.

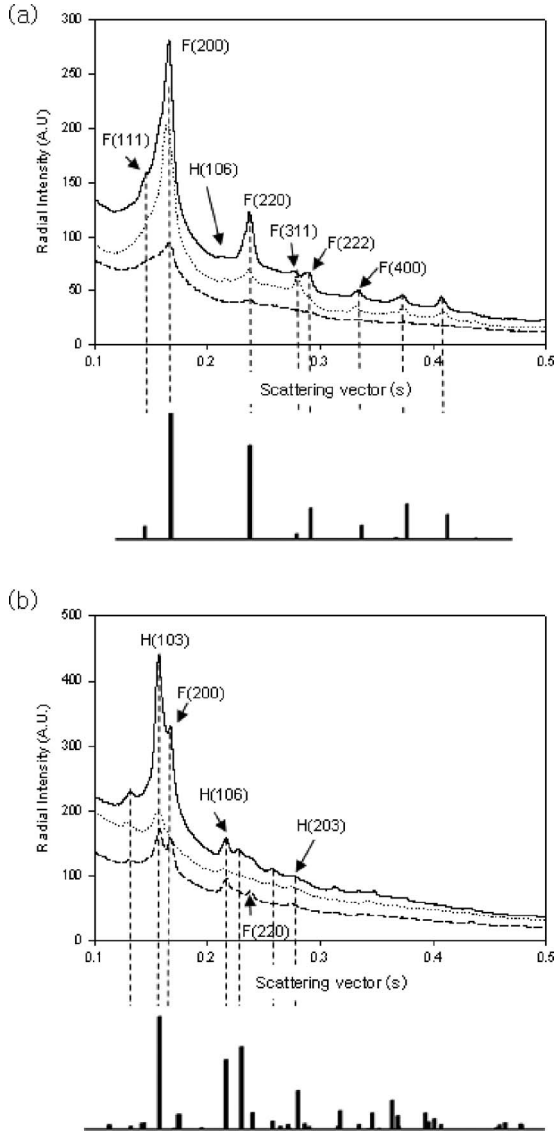

FIG. 4. Diffraction peaks from samples annealed at (a) 200 °C and (b) 100 °C with the simulated peaks of fcc and hexagonal $Ge_2Sb_2Te_5$. The x axis represents the scattering vector, defined by $\sin(\theta_B)\lambda$ where θ_B is the Bragg angle and λ is the wavelength of incident electrons accelerated at 200 kV.

TABLE I. Experimentally observed d spacings of nanoparticles and theoretical d spacings of fcc $Ge_2Sb_2Te_5$. The d spacing is related to the scattering vector as $d=\lambda/[2\sin(\theta_B)]=1/(2s)$.

fcc $Ge_2Sb_2Te_5$		Group III (200 °C)
(hkl)	$\sin\theta/\lambda$	$\sin\theta/\lambda$
(111)	0.144	0.144
(200)	0.166	0.166
		0.216
(220)	0.235	0.236
(311)	0.276	0.277
(222)	0.288	0.289
(400)	0.333	0.333

The major diffraction peaks observed in the sample annealed at 200 °C can be indexed based on the rocksalt structure with $a=6.01$ Å. The strong peak observed in the sample is from the {200} planes, which are used as a reference for indexing the diffraction peaks in Table I. The values of $s=\sin(\theta_B)/\lambda$ measured from the diffraction peaks show excellent correspondence with the fcc structure, except for the weak peak at $d=2.2$ Å which comes from a few diffraction spots we saw in the recorded diffraction patterns. [This peak is indicated by the dashed arrow in Fig. 3(c).] This peak does not fit with the rocksalt structure of $Ge_2Sb_2Te_5$. Similar diffraction spots are also found in other areas of the sample. Thus, the frequency of occurrence is not negligible. The $d=2.2$ Å peak is close to the position of the (106) reflection of the hexagonal $Ge_2Sb_2Te_5$. These peaks are very strong in the sample annealed at 100 °C, as described in the next paragraph. The existence of the hexagonal (106) reflection thus indicates the minor presence of the hexagonal phase at this annealing temperature.

The diffraction patterns obtained from the sample annealed at 100 °C, on the other hand, show substantial discrepancies with the fcc structure. More diffraction peaks were observed than for the group III samples. The spots at $d=2.2$ Å, which appeared weakly in the group III samples, are now a major diffraction peak, as shown in Fig. 4(b). To index the diffraction pattern, we calculated the d-spacing ratios using the strong (103) peak as the reference, and they are shown in Table II. Overall, the d-spacing ratios are in close agreement with the stable hexagonal structure [see Fig. 4(b) and Table II]. The agreement of the measured d spacings ($d=1/2s$, s values are listed in the table) with the calculated ones based on the hexagonal structure of $a=4.2$ Å and $c=16.96$ Å,[16] however, is not as good as that which was obtained for the sample annealed at 200 °C or that for the fcc structure. Better agreement is obtained if we expand the lattice constants by 6%, while keeping the a/c ratio constant.

TABLE II. Experimentally observed d spacings of nanoparticles and theoretical d spacings of hexagonal $Ge_2Sb_2Te_5$. The lattice constants for the hexagonal structure used in the table are $a=4.2$ Å and $c=16.96$ Å (Ref. 18). The listed reflections have relatively large structure factors except for (100) in the hexagonal structure. The d spacing is related to the scattering vector as $d=\lambda/[2\sin(\theta_B)]=1/(2s)$. The hexagonal (103) reflection is used as the reference to calculate the d-spacing ratios which are then used for indexing.

Hexagonal $Ge_2Sb_2Te_5$			Group II (100 °C)	
(hkl)	$\sin\theta/\lambda$	$d(103)/d(hkl)$	Scattering vector	$d(103)/d(hkl)$
(100)	0.137	0.840	0.132	0.84
(103)	0.163	1.000	0.157	1.00
			0.166	1.06
(106)	0.223	1.371	0.215	1.37
(110)	0.238	1.457	0.226	1.44
(107)	0.248	1.517	0.237	1.51
(009)	0.265	1.623	0.257	1.64
(203)	0.289	1.767	0.276	1.76

This is shown in Fig. 4(b). We have also tried two other reported lattice constants[19,20] but the agreement did not improve.

In the sample annealed at 100 °C, the strong fcc {200} peak and the fcc {220} peak are also observed. This indicates the coexistence of the fcc and hexagonal phases at this processing temperature. The other discrepancy we observed with the hexagonal structure is the spots at the scattering vector corresponding to $d=3.8$ Å at the position of the hexagonal {100} peak. However, no other {h00} peaks with larger calculated structure factors are present in the diffraction patterns, so it is not clear whether the peak at $d=3.8$ Å can be indexed as hexagonal {100} nor can we rule out the possibility that this peak comes from a minor phase.[21]

Figure 5 shows the reduced RDF obtained from each sample. The radial distribution function gives the distance correlation between a pair of atoms. According to Ref. 22, the RDF is calculated by

$$rG(r) = 4\pi r^2[\rho(r) - \rho_0] = \frac{2r}{\pi}\int_0^\infty S\left[\frac{I(S)}{Nf^2} - 1\right]\sin rSdS, \tag{1}$$

where $\rho(r)$ is the reduced density, which corresponds to the number of atoms per unit volume at a distance r from the reference atom, and $4\pi r^2\rho(r)dr$ is the number of atoms contained in a spherical shell of radius r and thickness dr. The other quantities involved in Eq. (1) are ρ_0, which is the average density of atoms in the sample, $S=4\pi\sin\theta/\lambda$, $I(S)$ the recorded electron diffraction intensity minus the inelastic background, and N the normalization factor. $\langle f\rangle$ is the averaged atomic scattering factor given by $\langle f\rangle=\Sigma_i c_i K_i f$, where the assumption is made that the atomic scattering is proportional to the atomic number. The value of f is determined from $\langle f^2\rangle=\Sigma_i c_i f_i^2=\Sigma_i c_i K_i^2 f^2$ and $f_i=\Sigma_i c_i\int_0^\infty 4\pi r^2 V_i(r)\times(\sin Sr/Sr)dr$ where V is the atomic potential and c_i the concentration. The RDF provides information on the distances between the atoms, as well as the averaged coordination numbers. The results of the RDF analysis are shown in Fig. 5. The diffraction patterns used for the RDF analysis were recorded by minimizing the contribution from the nanocrystals. The main diffraction spots from the nanocrystals were deleted from the diffraction patterns before the RDF analysis. The accuracy of the RDF analysis was checked by comparing the results from two different areas of the samples. The peak shapes and intensities are similar and the peak positions are reproducible within a distance of 0.1 Å. The method itself was tested in the analysis of other amorphous structures.[23] The first nearest neighbor distances are similar for the as-prepared film and the film annealed at 100 °C, with the film annealed at 200 °C showing a slightly larger distance. This agrees with the previously reported extended X-ray absorption fine structure (EXAFS) results of an amorphous GST film.[24] Kolobov *et al.* showed that the bonding distance in the amorphous area is shorter than that in the fcc crystalline area. Considering that the samples in group III have a more highly crystalline phase, a small shift of the first peak toward the crystalline value in group III is reasonable.

The next peak at ~4.1 Å in all three groups is associated with the short Te–Te bonding, whose length is 4.27 Å in the case of the fcc or 4.2 Å in the case of the hexagonal structure. After this peak, there are significant differences in both the peak position and shape. In the case of the fcc structure, peaks at 5.2, 6.2, and 6.9 Å are expected. The last two are observed experimentally in the annealed samples. A somewhat shorter distance of 4.9 Å is observed in the samples annealed at 200 °C. Thus, by comparing these structures with the amorphous ones, it can be inferred that the nanopar-

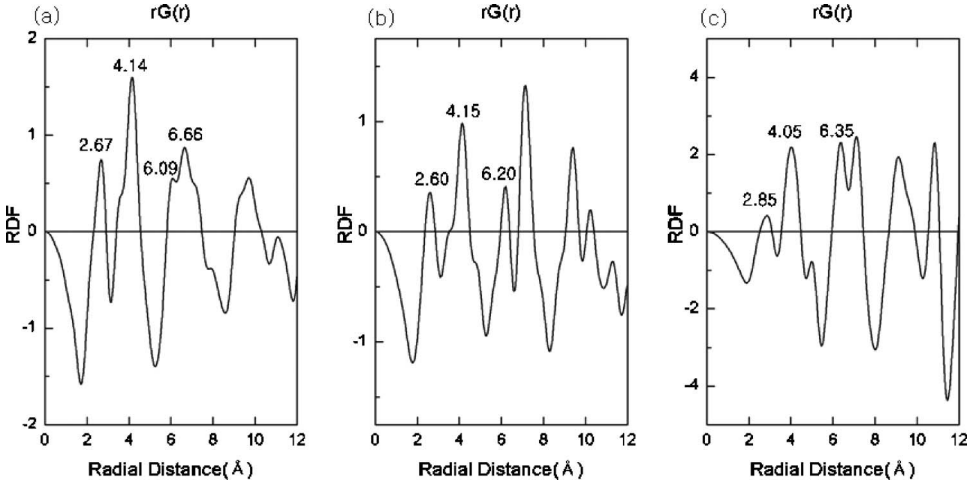

FIG. 5. Radial distribution functions calculated from the experimental diffraction patterns of the $Ge_2Sb_2Te_5$ nanoparticles (a) as-prepared at room temperature and annealed at (b) 100 °C and (c) 200 °C.

ticles in the group III samples are crystallized mostly with the fcc $Ge_2Sb_2Te_5$ structure, and the surrounding amorphous phase has similar short range atomic arrangements as these crystalline phases.

Apart from the major peaks identified above, unexpected shoulders are also observed, especially in the as-prepared sample and the sample annealed at 100 °C. For example, the shoulder at 3.4 Å is reproducible. There is a similar Te–Te bonding distance near the center in the hexagonal structures, which was reported to be 3.61 Å (Ref. 18) or 3.75 Å.[20] The intensities of these peaks can vary in different areas.

IV. CONCLUSIONS

In summary, the structures of the as-prepared GST nanoparticles and those annealed at 100 and 200 °C were studied by electron diffraction. The first and second nearest neighbor distances of the amorphous structures of the group III samples are almost the same as those reported by Kolobov *et al.* while the second peaks in groups I and II samples are somewhat different from those reported in a previous publication.[24] The hexagonal structure is dominant in the sample annealed at 100 °C. A substantial amount of the fcc structure as the second phase is also observed in this sample. In comparison, most of the nanocrystals annealed at 200 °C have the fcc $Ge_2Sb_2Te_5$ structure and only a very small fraction of hexagonal $Ge_2Sb_2Te_5$ is observed.

ACKNOWLEDGMENTS

This work was supported by Grant No. R01-2006-000-11071-0 from the Basic Research Program of the Korea Science and Engineering Foundation. Two of the authors (H.R.Y. and W.J.) are also supported by a Korea Research Foundation grant (MOEHRD and KRF-2005-041-C00165) and by a grant (Code No. 07K1501-02520) from the "Center for Nanostructured Materials Technology" under the "21st Century Frontier R&D Programs" of the Korean Ministry of Science and Technology. Electron microscopy was carried out using the facility of the Center for Microanalysis of Materials at FS-MRL, University of Illinois Urbana-Champaign, which is partially supported by DEFG02-91ER45439.

[1] S. Lai and T. Lowrey, Tech. Dig. - Int. Electron Devices Meet. **2001**, 803.
[2] S. Lai, Tech. Dig. - Int. Electron Devices Meet. **2001**, 255.
[3] M. Grill, T. Lowrey, and J. Park, *Proceeding of the 2002 IEEE International Solid State Circuits Conference* (IEEE, New York, 2002), Vol. 2, p. 158.
[4] M. B. Luo and M. Wuttig, Adv. Mater. (Weinheim, Ger.) **16**, 439 (2004).
[5] I. Friedrich, V. Weidenhof, W. Njoroge, P. Franz, and M. Wuttig, J. Appl. Phys. **87**, 4130 (2000).
[6] J. Maimon, E. Spall, R. Quinn, S. Schnur, Proceedings of the IEEE 2001 Aerospace Conference, 2001, Vol. 5, p. 2289.
[7] A. L. Lacaita, A. Redaelli, D. Ielmini, F. Pellizzer, A. Pirovano, A. Benvenuti, and R. Bez, Tech. Dig. - Int. Electron Devices Meet. **2004**, 911.
[8] Y. H. Ha, J. H. Yi, H. Horii, J. H. Park, S. H. Joo, S. O. Park, U.-I. Chung, and J. T. Moon, Tech. Dig. VLSI Symp. **2003**, 175.
[9] F. Pellizzer *et al.*, Tech. Dig. VLSI Symp. **2004**, 18.
[10] S. J. Ahn *et al.*, Tech. Dig. VLSI Symp. **2005**, 98.
[11] G. H. Koh *et al.*, IEEE International Conference on IC Design and Technology, 2004 (unpublished).
[12] T. A. Lowery *et al.*, MRS Fall Meeting, 2003, p. HH2.1.
[13] H. R. Yoon, W. Jo, E. H. Lee, M. Kim, J. H. Lee, K. Y. Lee, and Y. Khang, J. Non-Cryst. Solids **351**, 3430 (2005).
[14] D.-S. Suh *et al.*, Appl. Phys. Lett. **90**, 023101 (2007).
[15] J. M. Zuo, M. Gao, J. Tao, B. Q. Li, R. Twesten, and I. Petrov, Microsc. Res. Tech. **64**, 347 (2004).
[16] H. R. Yoon, W. Jo, E. Cho, S. Yoon, and M. Kim, J. Non-Cryst. Solids **352**, 3757 (2006).
[17] N. Yamada and T. Matsunaga, J. Appl. Phys. **88**, 7020 (2000).
[18] I. I. Petrov, R. M. Imamov, and Z. G. Pinsker, Sov. Phys. Crystallogr. **13**, 339 (1968).
[19] B. J. Kooi and J. Th. M. De Hosson, J. Appl. Phys. **92**, 3584 (2004).
[20] T. Matsunaga, N. Yamada, and Y. Kubota, Acta Crystallogr., Sect. B: Struct. Sci. **B60**, 685 (2004).
[21] N. Yamada, E. Ohno, K. Nishiuchi, N. Akahira, and M. Takao, J. Appl. Phys. **69**, 2848 (1991).
[22] D. J. H. Cockayne and D. R. McKenzie, Acta Crystallogr., Sect. A: Found. Crystallogr. **A44**, 870 (1988).
[23] H. Chen and J. M. Zuo, Acta Mater. **55**, 1617 (2007).
[24] A. Kolobov, R. Fons, A. I. Frenkel, A. L. Ankudinov, J. Tominaga, and T. Uruga, Nat. Mater. **3**, 703 (2004).